# High resolution x-ray diffraction study of smectic polymorphism and fluctuations in a mixture of octyl- and decyl-oxyphenyl nitrobenzoyloxy benzoate

Yushan Shi,[1] George Nounesis,[2] Carl W. Garland,[3] and Satyendra Kumar[1]
[1]*Department of Physics and Liquid Crystal Institute, Kent State University, Kent, Ohio 44242*
[2]*Institute of Radioisotopes and Radiodiagnostic Products, NCSR "Demokritos," Aghia Paraskevi, Attiki, Greece*
[3]*Department of Chemistry, Massachusetts Institute of Technology, Cambridge, Massachusetts 02139*
(Received 20 June 1997)

Reentrant nematic phases and smectic antiphases occur as intermediate states between two one-dimensionally ordered frustrated smectic phases, characterized by two competing and, in general, incommensurate smectic density waves. Using high-resolution x-ray diffraction, we have examined the evolution of the two density waves as a function of temperature in all phases of a mixture of polar liquid crystals octyl- and decyl-oxyphenyl nitrobenzoyloxy benzoate (47.4 mol% $DB_8ONO_2$+52.6% $DB_{10}ONO_2$). This mixture exhibits at temperatures below 127 °C the liquid-crystal phase sequence: smectic-$A_d$, reentrant nematic phases $N_d$ and $N_1$, smectic-$A_1$, tilted antiphase $\tilde{C}$, smectic-$A_2$, and smectic-$C_2$ phases. Detailed investigations of several order-disorder transitions and the evolution of fluctuation effects in this system are reported. [S1063-651X(97)04411-5]

PACS number(s): 61.30.−v, 61.10.−i, 64.70.Md

## I. INTRODUCTION

The study of frustrated smectic phases, marked with two competing incommensurate length scales, has been an active field of research since the first observation in 1979 of phase transition between two optically identical smectic-$A$ phases [1]. Polymorphism and frustrations occur in smectic liquid crystals primarily due to the dipole-dipole interactions between polar molecules that can form antiferroelectric pairs or dimers [2]. The length of the molecular dimer, $l'$, is temperature dependent, and typically $l' \sim (1.4-1.8)l$, where $l$ is the molecular length. Thus there are two competing lengths $l$ and $l'$, leading to three kinds of smectic-$A$ phases: a monolayer smectic-$A_1$ with layer thickness $d=l$, a bilayer smectic-$A_2$ with $d=2l$, and a partial bilayer smectic-$A_d$ with $l \leqslant d \leqslant 2l$. A phenomenological model for frustrated smectics was first proposed by Prost and co-workers [3]. This model has been very successful in explaining smectic polymorphism and predicting diverse phase diagrams and the existence of new phases. Two-dimensionally ordered phases with local smectic order, denoted as the antiphase $\tilde{A}$ and the tilted antiphase $\tilde{C}$, have been observed [4–6], and are two of the phases predicted as a consequence of an escape from incommensurability between the two density waves. A fluctuation-corrected model for frustrated smectics developed by Prost and Toner [7] predicted the existence of a reentrant nematic region surrounded by smectic phases. Their model also indicated that at a smectic-smectic critical point, the smectic-layer compressibility would vanish and the entropy would increase dramatically to unbind dislocation loops. Positional order was thus lost and a smectic phase therefore melted into a nematic phase. The phase diagrams based on the new model present a remarkable variety of topologies, one of which is in agreement with the observed nematic "estuary" flanked by the smectic-$A_d$ (Sm-$A_d$) and smectic-$A_1$ (Sm-$A_1$) "coasts" in mixtures of octyl-oxyphenyl nitrobenzoyloxy benzoate ($DB_8ONO_2$) and decyl-oxyphenyl nitrobenzoyloxy benzoate ($DB_{10}ONO_2$) [8]. A microscopic model developed by Berker and co-workers [9] also provides a theoretical frustrated-smectic phase diagram in very good agreement with the experimental $DB_8ONO_2$ and $DB_{10}ONO_2$ phase diagram. One very interesting aspect of the Prost-Toner model [7] is the prediction that a smectic-smectic critical point will be replaced by a nematic region ("lake") with an associated liquid-gas-like critical point between two uniaxial nematics. A first-order phase transition between the two predicted nematics, $N_d$ and $N_1$, characterized by Sm-$A_d$ and Sm-$A_1$ short range order, respectively, has been discovered recently with high resolution ac calorimetric and x-ray diffraction techniques [10].

Mixtures of the polar liquid crystals $DB_8ONO_2$ and $DB_{10}ONO_2$ are one of the classic systems of frustrated smectics and have been studied using various experimental methods [8,10–12]. Its temperature-concentration ($T$-$X$) phase diagram has been well documented in the literature [8,10–12]. In the nematic "estuary," a Sm-$A_d$−Sm-$A_1$−$N$ triple point is located approximately at $T$=125.5 °C and $X$=55, where $X$ denotes the *mole* percentage of $DB_{10}ONO_2$. In previously reported work, a mixture with $X$=52.6 was studied to provide calorimetric and x-ray evidence of a nematic-nematic phase transition [10] and x-ray evidence for the onset and evolution of the tilted smectic antiphase $\tilde{C}$ [12]. Here, we present results of a comprehensive study of the fluctuation effects in frustrated smectics. In this paper, we will first present the x-ray confirmation of the uniaxial Sm-$A_d$−$N_d$−$N_1$−Sm-$A_1$ phase sequence in more detail and demonstrate the evolution of the two incommensurate smectic density waves as a function of temperature. We then discuss the onset and evolution of the tilted antiphase $\tilde{C}$ between the Sm-$A_1$ and smectic-$A_2$ (Sm-$A_2$) phases. The transition from the Sm-$A_1$ phase with short range partial bilayer order to the antiphase $\tilde{C}$ has been analyzed by analogy to the transition between Sm-$A$-like and Sm-$C$-like fluctuations in the Chen-Lubensky model [13]. Furthermore, we have closely examined the undulation and tilting of smectic layers at the onset of the tilted antiphase $\tilde{C}$ and determined completely the structural evolution and fluctuation effects from the Sm-$A_d$ phase to the Sm-$A_2$ phase.

## II. EXPERIMENTAL DETAILS

The alkoxyphenyl nitrobenzoyloxy benzoates, denoted as $DB_nONO_2$, have the general chemical formula

$$C_nH_{2n+1}O\text{–}\phi\text{–}OOC\text{–}\phi\text{–}OOC\text{–}\phi\text{–}NO_2\,,$$

where $\phi$ denotes the benzene ring and $n$ is the number of carbons in the alkyl chain. Pure $DB_9ONO_2$ exhibits the following sequence of phase transitions on cooling at atmospheric pressure [14]: $I-(224\,°C)-N-(195\,°C)-\text{Sm-}A_d'-(152\,°C)-N_r-(134.6\,°C)-\text{Sm-}A_d-(124\,°C)-N_r-(121.6\,°C)-\text{Sm-}A_1-(119\,°C)-\tilde{C}-(100\,°C)-\text{Sm-}A_2-(96\,°C)-\text{Sm-}C_2$. The symbol $I$ denotes the isotropic phase, and the subscript $r$ denotes the reentrant nematic phase. A binary $DB_8ONO_2+DB_{10}ONO_2$ mixture with $X=52.6$ exhibits the same phase sequence as $DB_9ONO_2$. Partial phase diagrams for this system adapted from Ref. [14] and Ref. [10] are shown in Fig. 1. Approximately 100 mg of the $X=52.6$ mixture was placed between two 8 $\mu$m thick Mylar sheets and mounted in an oven that provided a thermal stability of $\pm0.01$ K. The sample was chemically stable over two months. A magnetic field of 0.65 T was produced by a pair of rare-earth permanent magnets with tapered pole faces, as shown in Fig. 2. These magnets were installed inside the oven to ensure good alignment during the experiment.

The experiment was conducted using a four-circle x-ray diffractometer with a copper rotating anode source and two germanium single crystals [(111) surface] as monochromator and analyzer in a nondispersive setup. Cu $K\alpha$ characteristic radiation was selected and the wavelength of the incident x-ray beam was 1.54178 Å ($K\alpha$ doublet was not resolved in this experiment). The power of the x-ray generator was held constant at 15 kW. A pair of slits was placed 135 mm before the sample to define the size of the incident beam to a dimension of 1.5 mm in horizontal and 6.0 mm in vertical directions, respectively. The resolution of the diffractometer was $\sim4\times10^{-4}$ Å$^{-1}$ in the longitudinal direction, $\sim4\times10^{-5}$ Å$^{-1}$ in the transverse in-plane direction, and $\sim2\times10^{-2}$ Å$^{-1}$ in the direction perpendicular to the scattering plane. Two Na(Tl)I scintillation detectors were used to measure the scattered beam intensity and to monitor the incident x-ray flux. A thin sheet of Kapton placed in the evacuated beam line before the sample scattered a small portion of the incident radiation vertically into the monitor. The intensity of the scattered beam was normalized against the monitor counts to remove any possible effects of power fluctuations in the source. To assure high resolution in the data, the *zone mode* of four-circle geometry [15] was used to perform both linear and mesh scans in the scattering plane. The structure and texture of the sample in the out-of-plane directions were examined with $\chi$ and $\phi$ scans.

The sample was aligned by first heating to the high-temperature nematic phase (above 200 °C) and then in the

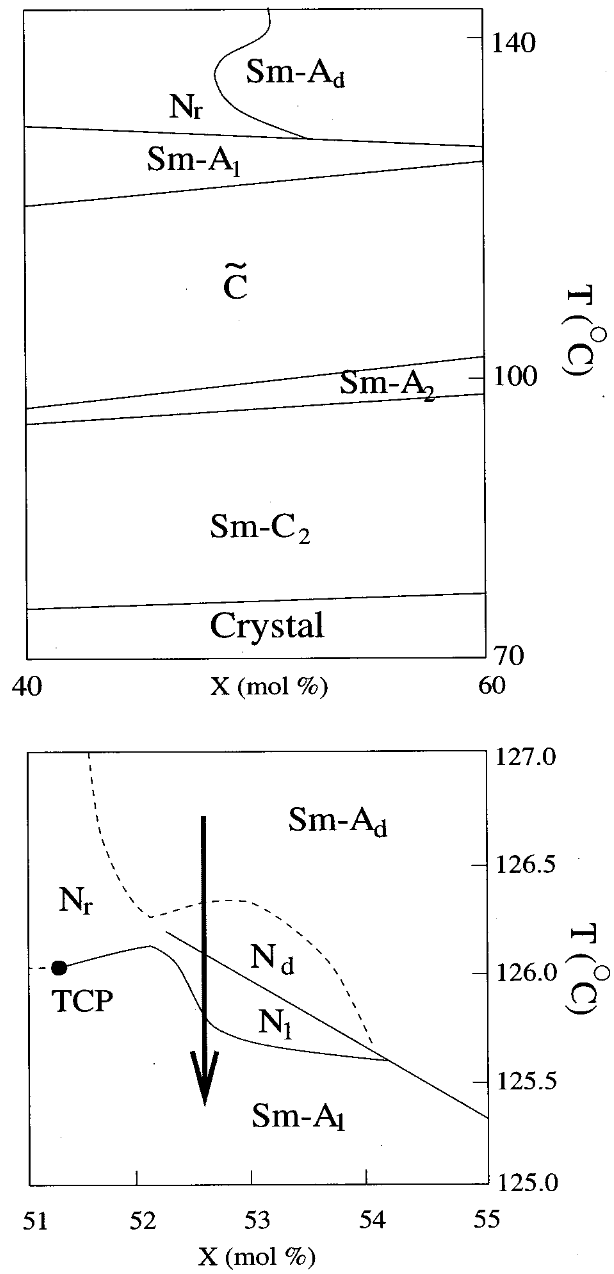


FIG. 1. Partial phase diagrams for $DB_8ONO_2+DB_{10}ONO_2$ mixtures adapted from Ref. [14] (upper panel) and Ref. [10] (lower panel). The downward arrow represents the $X=52.6$ mixture used in the present study. TCP shows the location of a tricritical point.

reentrant $N_r$ phase ($T=125.9\,°C$) with the help of *in situ* magnetic field. To improve the alignment, the sample was cycled through the reentrant nematic phase by changing the sample temperature between 134 °C (Sm-$A_d$ phase) and 125.8 °C ($N_r$ phase) three or four times. The intensity and full peak widths at half maximum (FWHM) of the condensed Sm-$A_d$ peak were 38 000 per 100 000 monitor counts (or 6400 counts/sec), $\Delta2\theta=0.011°$, and $\Delta\omega=2.0°$. Alignment of the molecules was initially symmetric with respect to the $Q_z$ axis ($z$ being parallel to the director) and nearly perfect. The minimum mosaic width of the condensed Sm-$A_1$ Bragg peaks was $\Delta\omega=1.6°$ measured just below the $N_r$-Sm-$A_1$

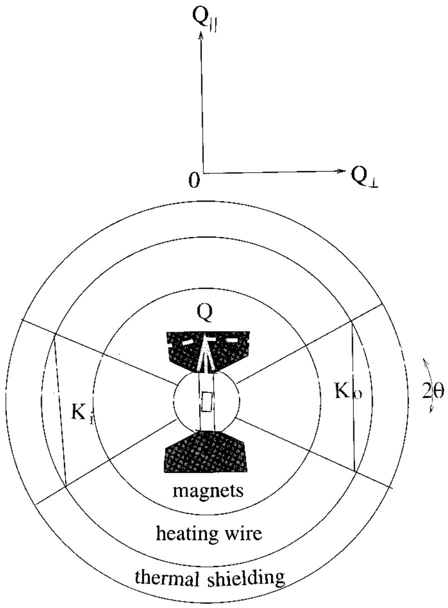


FIG. 2. The sample was mounted inside the oven and aligned with an *in situ* magnet field. The x-ray wave vectors $K_i$ and $K_o$ were defined by the incident beam and position of detector. $2\theta$ is the scattering angle and **Q** is the scattering vector. $Q_\parallel$ is the component of **Q** parallel to the long axis of the molecules defined by the magnetic field, and $Q_\perp$ is the perpendicular component.

transition temperature. The shape of the Sm-$A_1$ Bragg peak indicated excellent alignment of the sample, almost as good as a single crystal.

## III. RESULTS AND DISCUSSION

### A. Uniaxial phase sequence: Sm-$A_d$−$N_d$−$N_1$−Sm-$A_1$

Figure 3 shows the diffraction patterns in the Sm-$A_d$, $N_d$, $N_1$, and Sm-$A_1$ phases, which clearly illustrated the competition between two collinear but incommensurate wave vectors corresponding to lengths $d_1 = 2\pi/2q_0$ and $d = 2\pi/q'$. The two scattering peaks at $2q_0$ and $q'$ in all phases, either condensed or diffused, are symmetric with respect to the $Q_\parallel$ direction defined by an external magnetic field. At 126.51 °C in the Sm-$A_d$ phase the $q'$ scattering was condensed into a quasi-Bragg peak at (0, 0, 0.1365) Å$^{-1}$, while the $2q_0$ scattering was diffuse around (0, 0, 0.2034) Å$^{-1}$ with two orders of magnitude lower peak intensity, 4 times wider in $Q_\parallel$ and ~10 times wider in $Q_\perp$ directions than those of the $q'$ peak. The position, intensity, and widths of both $2q_0$ and $q'$ peaks as a function of temperature are listed in Table I. The smectic layer spacing was 46.0 Å at this temperature in the Sm-$A_d$ phase. Ten evenly spaced iso-intensity contours are plotted for each peak in Fig. 3, indicating the nature of condensed and diffuse scatterings corresponding to the two incommensurate density waves.

At a temperature (125.7 °C) in the Sm-$A_1$ phase, shown in Fig. 3(d), the situation was reversed. Scattering at $2q_0$ condensed into a quasi Bragg peak, while $q'$ scattering became diffuse. The smectic layer spacing in the Sm-$A_1$ phase was 30.9 Å. The ratios of the peak intensities and the integrated intensities for $q'$ to $2q_0$ peaks were 86 and 2, respectively (after the correction for the Lorentz-polarization factor) in the Sm-$A_d$ phase, 1/73 and 0.45 in the Sm-$A_1$ phase, respectively. The drastic change of maximum intensities of $2q_0$ and $q'$ peaks from Sm-$A_d$ to Sm-$A_1$ phases is associated with the dramatic change in the Sm-$A_d$ and Sm-$A_1$ susceptibilities, while a small change in the ratio of integrated intensities of $q'$ to $2q_0$ peaks is primarily due to the ratio of form factors.

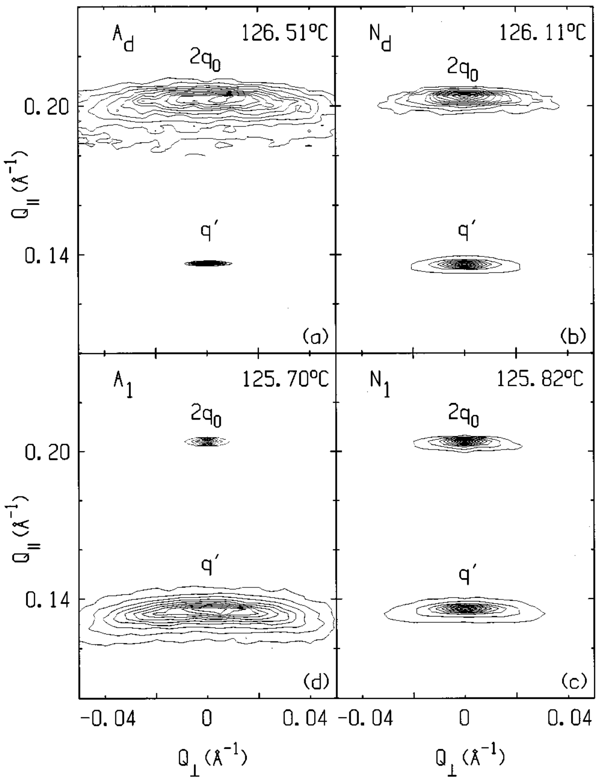


FIG. 3. Competing monolayer and partial bilayer fluctuations in the uniaxial Sm-$A_d$, $N_d$, $N_1$, and Sm-$A_1$ phases. Ten evenly spaced iso-intensity contours are plotted for each peak.

In a narrow range of ~0.8 K between the Sm-$A_d$ and Sm-$A_1$ phases, the two nematic phases, $N_d$ and $N_1$ shown in Figs. 3(b) and 3(c), have been identified previously [10,11] in agreement with the fluctuation-corrected mean-field theory of frustrated smectics proposed by Prost and Toner [7]. The confirmation of a first-order transition between these two uniaxial nematic phases has already been reported [10]. Both $q'$ and $2q_0$ peaks were diffuse [Figs. 3(b) and 3(c)] indicating the absence of quasi-long range positional order. The two nematics differ in the nature of dominant smectic fluctuations. Sm-$A_d$ fluctuations dominate in the $N_d$ phase and Sm-$A_1$ fluctuations dominate in the $N_1$ phase. In the $N_d$

TABLE I. The position, intensity per 100 000 monitor counts and widths of $2q_0$ and $q'$ peaks at Sm-$A_d$ and Sm-$A_1$ phases.

| Peak | $T$ (°C) | $Q$ (Å$^{-1}$) | $\Delta Q_\parallel$ (Å$^{-1}$) | $\Delta Q_\perp$ (Å$^{-1}$) | Intensity |
|---|---|---|---|---|---|
| $q'$ | 126.51 | 0,0,0.1365 | 0.0007 | 0.005 | 38 000 |
| $2q_0$ | 126.51 | 0,0,0.2034 | 0.0028 | 0.054 | 200 |
| $q'$ | 125.70 | 0,0,0.134 | 0.012 | 0.08 | 422 |
| $2q_0$ | 125.70 | 0,0,0.2034 | 0.0009 | 0.0065 | 14 000 |

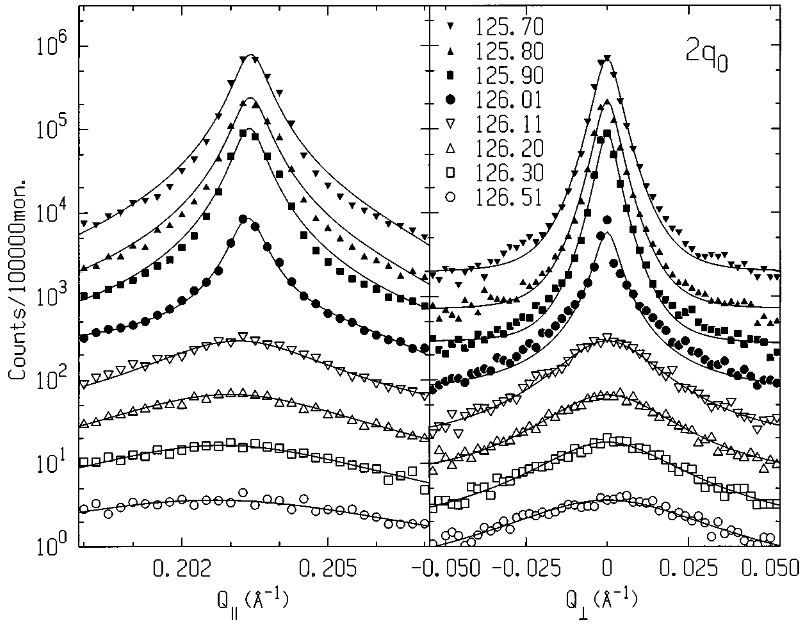


FIG. 4. Longitudinal ($Q_\parallel$) and transverse ($Q_\perp$) scans of the monolayer ($2q_0$) peak in the Sm-$A_d-N_d-N_1-$Sm-$A_1$ phase sequence. The transverse scans were performed at the $Q_\parallel$ peak positions observed in longitudinal scans. The data and the fits have been shifted vertically for clarity.

phase at 126.11 °C, the susceptibility and the longitudinal and transverse correlation lengths of Sm-$A_d$ fluctuations are more than one order of magnitude stronger than those of Sm-$A_1$ fluctuations. On the other hand, in the $N_1$ phase at 125.82 °C, the dominant fluctuations are due to short-range Sm-$A_1$ order. The ratio of the two incommensurate lengths in this system is about 1.49 according to the positions of the $q'$ and $2q_0$ peaks in the two reentrant nematic phases.

The temperature dependence of smectic correlations near the two transitions from one of the nematics to the neighboring smectic phase were determined by analyzing the line shape using the empirical [13] form

$$S(q)=\frac{\sigma}{1+B(Q_\parallel-Q_0)^2+CQ_\perp^2+DQ_\perp^4}, \tag{1}$$

convoluted with the resolution function. Here $\sigma$ is the smectic susceptibility, $Q_\parallel$ the longitudinal, and $Q_\perp$ the transverse component of the scattering vector. $Q_0$ represents the peak position along the $Q_\parallel$ axis, which could be either $q'$ or $2q_0$. The coefficients $B$, $C$, $D$ are adjustable parameters determined by the correlation lengths and the type of smectic fluctuations. The value of $C$ is positive for uniaxial and negative for biaxial fluctuations [13]. While traversing the Sm-$A_d-N_d-N_1-$Sm-$A_1$ phase sequence on cooling, both longitudinal and transverse scans of the two peaks, $2q_0$ and $q'$, were conducted at 0.05 K intervals. Figure 4 and Fig. 5 present the $2q_0$ and $q'$ peaks and their fits to Eq. (1). Only every other scan has been shown in these figures, and the scans have been vertically shifted for the sake of clarity. The solid curves represent the best fits.

Following Martinez-Miranda, Kortan, and Birgeneau [16], the correlation lengths $\xi_\parallel$ and $\xi_\perp$ for both uniaxial and biaxial smectic fluctuations can be calculated from the parameters obtained from the fits, as follows:

$$\xi_\parallel=\begin{cases}\left[\dfrac{B}{1+\frac{1}{2}C(Q_\perp^0)^2}\right]^{1/2}, & C<0\\ \sqrt{B}, & C>0\end{cases} \tag{2}$$

and

$$\xi_\perp=\begin{cases}\dfrac{\sqrt{2D}}{\{-C+[C^2+4D(1-C^2/2D)]^{1/2}\}^{1/2}-\sqrt{-C}}, & C<0\\ \left[\dfrac{2D}{-C+(C^2+4D)^{1/2}}\right]^{1/2}, & C>0,\end{cases} \tag{3}$$

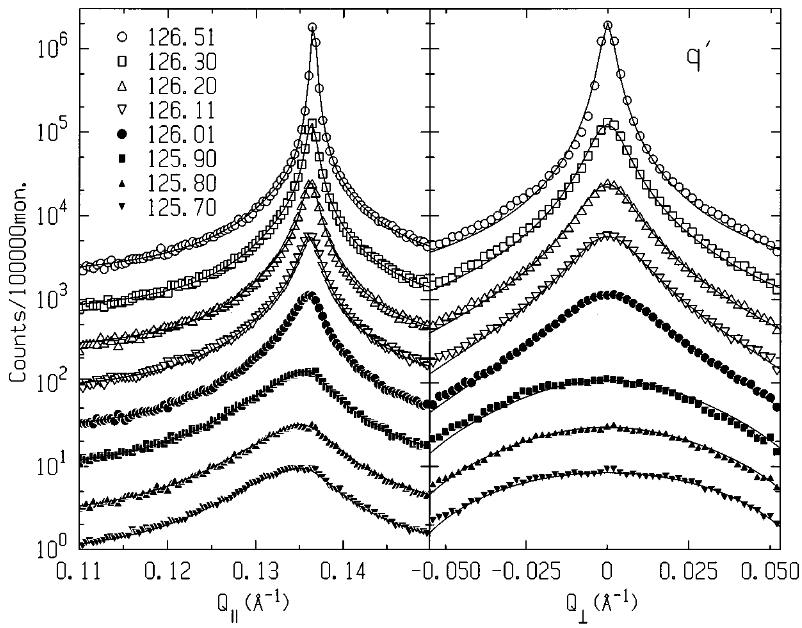


FIG. 5. Longitudinal and transverse scans of the partial bilayer ($q'$) peak in the Sm-$A_d$, $N_d$, $N_1$, and Sm-$A_1$ phases. The transverse scans were performed at the $Q_\parallel$ peak positions observed in longitudinal scans. The data and fit curves have been shifted vertically for clarity.

where $Q_\perp^0$ is the peak position along the $Q_\perp$ axis. In the uniaxial phase sequence where $Q_\perp^0=0$, the parameter $C$ is positive. The values of the correlation lengths $\xi_\parallel$ and $\xi_\perp$ for the uniaxial phase sequence are summarized in Fig. 6. The first order $N_d$-$N_1$ phase transition is evident from the jump in $\xi_\parallel$ and $\xi_\perp$ of the Sm-$A_1$ order and a sharp change in slopes of $\xi_\parallel$ and $\xi_\perp$ plots belonging to the Sm-$A_d$ order at 125.97 °C. A description of the smectic susceptibilities and short-range layer spacings as functions of temperature at the first order nematic-nematic phase transition has been reported previously [10].

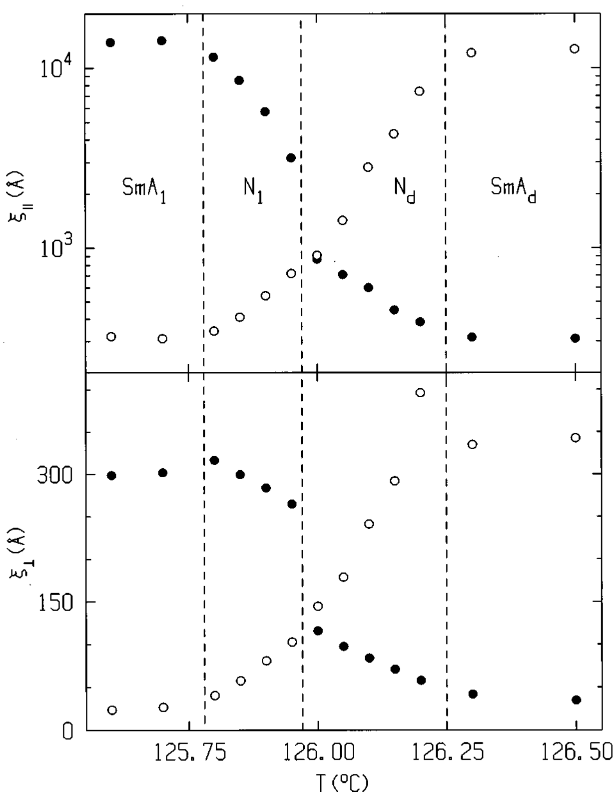


FIG. 6. Evolution of correlation lengths, $\xi_\parallel$ and $\xi_\perp$ of partial bilayer (Sm-$A_d$, open circles) and monolayer (Sm-$A_1$, full circles) smectic order in the Sm-$A_d$, $N_d$, $N_1$, and Sm-$A_1$ phases.

### B. Fluctuations in the Sm-$A_1$ phase

#### *1. Partial bilayer and antiphase fluctuations*

Below the $N_1-$Sm-$A_1$ transition temperature (125.8 °C), upon cooling from 125.5 °C to 124.5 °C, the condensed $2q_0$ peak became only slightly broader in the $Q_\perp$ direction due to a mild increase in mosaicity. But the changes in the diffuse $q'$ peak were pronounced. Figure 7 shows the profiles of the $q'$ peak in both longitudinal ($Q_\parallel$) and transverse ($Q_\perp$) directions as a function of temperature. For clarity, only every other data set is shown. The solid curves are best fits to the data with Eq. (1). The $q'$ peak position shifted nearly linearly from 0.1357 Å$^{-1}$ at 125.5 °C to 0.1347 Å$^{-1}$ at 124.5 °C at a rate of 0.001 Å$^{-1}$ per K. The longitudinal correlation length $\xi_\parallel$ of partial bilayer Sm-$A_d$ fluctuations decreased at first and then remained nearly constant at a value of 220 Å below 125.3 °C, as shown in Fig. 8.

The transverse scans were performed through the center of the peak at each temperature during cooling. The parameter $C$ decreased linearly and remained positive above 124.85 °C. The transverse correlation length $\xi_\perp$ was nearly constant at 19 Å in this uniaxial fluctuation region for the partial bilayer short range order in the Sm-$A_1$ phase. As the temperature was lowered below 124.85 °C, $C$ became negative and $\xi_\perp$ started to increase, indicating the onset of antiphase fluctuations. This pretransitional region was previously identified as the Sm-$A_1'$ phase [17]. The value of the in-plane wave vector $q_\perp^0$ was found to be 0.026 Å$^{-1}$ at the Sm-$A_1-\widetilde{C}$ transition at 120.49 °C, yielding a value of 242 Å for the antiphase modulation, which is comparable to the

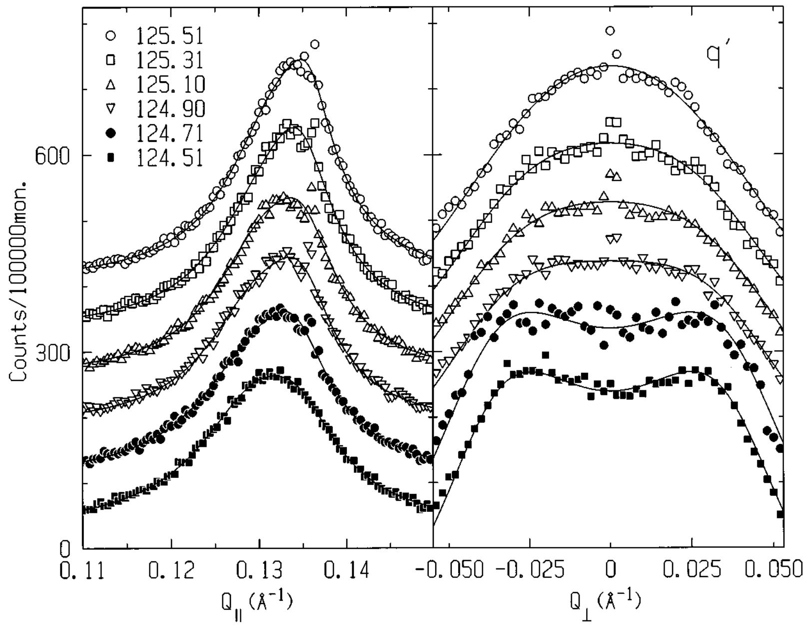


FIG. 7. Growth of biaxial fluctuations in the Sm-$A_1$ phase, as indicated by the diffuse scattering at $q'$. The $Q_\perp$ scans were performed at the peak positions found in longitudinal scans at different temperatures during cooling. Splitting of the $q'$ peak into a doublet in the transverse direction at lower temperature is evident. The peaks have been shifted vertically for clarity.

longitudinal correlation length, rather than the transverse correlation length, of the short-range partial bilayer (Sm-$A_d$-like) order at this temperature.

### *2. Smectic layer undulations*

The evolution of the $2q_0$ peak across the Sm-$A_1$–antiphase-$\widetilde{C}$ phase transition is shown in Fig. 9. High resolution $Q_\parallel$ and $Q_\perp$ scans with fine temperature steps were also performed for quantitative analysis. In the middle of the Sm-$A_1$ phase at 125.5 °C, the condensed quasi-Bragg peak was located at (0, 0, 0.204) Å$^{-1}$ with a nearly resolution limited FWHM of 0.0008 Å$^{-1}$ in $Q_\parallel$ and a minimum width of 0.0053 Å$^{-1}$ in the $Q_\perp$ direction. The orientational fluctuations increased upon cooling, which reflected a broadening due to sample mosaicity of the peak that was accompanied by a decrease in layer spacing. At $T=120.5$ °C, the mosaicity ($\Delta\omega$) of the Sm-$A_1$ domains and the fractional layer spacing change ($\Delta L/L$) attained the values of 8° and $-0.7$%, respectively. When temperature was decreased by 10 mK, at $T=120.49$ °C, two off-axis peaks appeared symmetrically at ($\pm 0.025$, 0, 0.204) Å$^{-1}$ superimposed on the on-axis peak with broad mosaicity. The off-axis peaks became sharp and intense without moving in $q$ space, and they grew at the expense of the intensity of the on-axis peak, indicating coexistence and an evolution from untilted to tilted smectic domains. The peak intensity at ($-0.025$, 0, 0.204) Å$^{-1}$ was about 1.5 times higher than at ($+0.025$, 0, 0.204) Å$^{-1}$, which is attributable to experimental geometry. The similarity of the shapes of the off-axis peaks in $\omega$ scans led us to conclude that the layers of the antiphase $\widetilde{C}$ were zigzag shaped with an angle of 14°, twice the molecular tilt of $\pm 7°$ [18]. Figure 10 shows the evolution of the $2q_0$ peak from the uniaxial smectic-$A_1$ phase to the biaxial tilted antiphase $\widetilde{C}$. The positions of on-axis and off-axis peaks are indicated by squares and circles, respec-

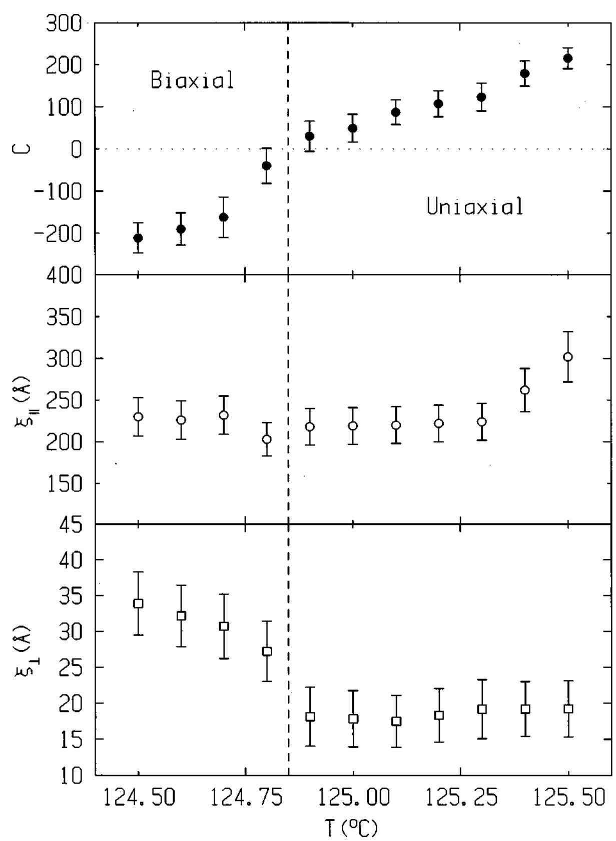


FIG. 8. The correlation lengths, $\xi_\parallel$ and $\xi_\perp$, and the fitting parameter $C$ (see text) for the $q'$ peak as a function of temperature near the uniaxial-biaxial transition of fluctuations. Near the transition, the longitudinal correlation length does not change noticeably, but the transverse correlation length changes from being nearly a constant in the ''uniaxial fluctuation'' region to values that monotonically increase on cooling into the ''biaxial fluctuation'' region.

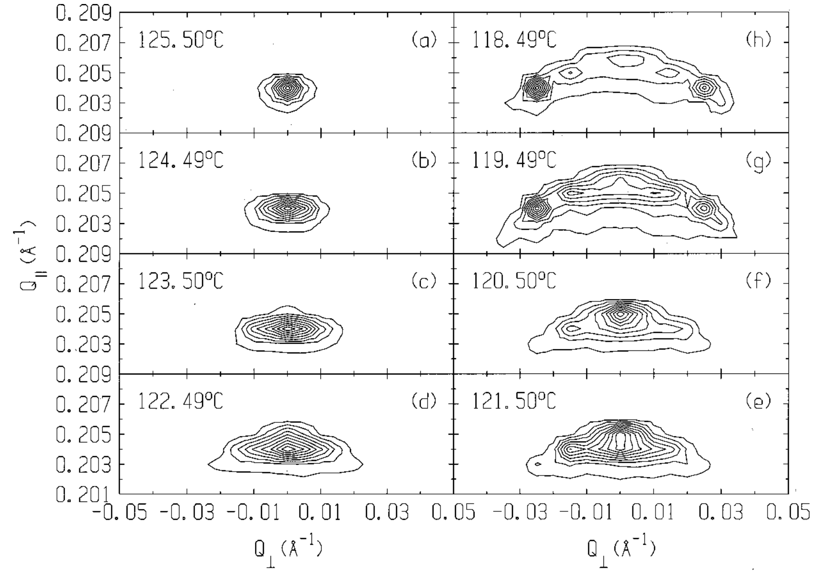


FIG. 9. Evolution of the $2q_0$ peak across the Sm-A$_1$–antiphase $\widetilde{C}$ transition. In the Sm-$A_1$ phase, right below the $N_1$ phase, the peak was on-axis and sharp. The peak became gradually broader and moved up slightly in $Q_\parallel$ upon cooling, mainly due to the development of undulations in the smectic layers. At the transition, which occurred at 120.49 °C, the off-axis doublet appeared, indicating the set of inplane density modulation associated with periodic tilt of smectic layers with respect to the director, which had been fixed in the $Q_\parallel$ direction by an external magnetic field.

tively. The vertical lines represent the full widths at half maximum in $\omega$ scans and the gray scale of the circles and squares represent qualitatively the intensity of the $2q_0$ peaks. As the temperature decreased, the magnitude of smectic layer undulation increased and turned into tilted domains of the $\widetilde{C}$ phase. In what follows, we discuss the details of only the off-axis peak at $(-0.025, 0, 0.204)$ Å$^{-1}$, referring to it as the $2q_0$ peak. The same description applies to the symmetric counterpart peak at $(+0.025, 0, 0.204)$ Å$^{-1}$.

### C. The Sm-$A_1$–$\widetilde{C}$–Sm-$A_2$–Sm-$C_2$ sequence

Growth of the antiphase modulation is primarily illustrated via the evolution of the $q'$ peak, as shown in Fig. 11. In the Sm-$A_1$ phase, Fig. 11(a), the diffuse $q'$ peak at (0, 0, 0.135) Å$^{-1}$ arises from the Sm-$A_d$ phase fluctuations which are incommensurate with the wave vector corresponding to the smectic-$A_1$ modulation. The onset of antiphase fluctuations became evident as two off-axis diffuse peaks began developing at 124.83 °C in the Sm-$A_1$ phase [17]. This off-

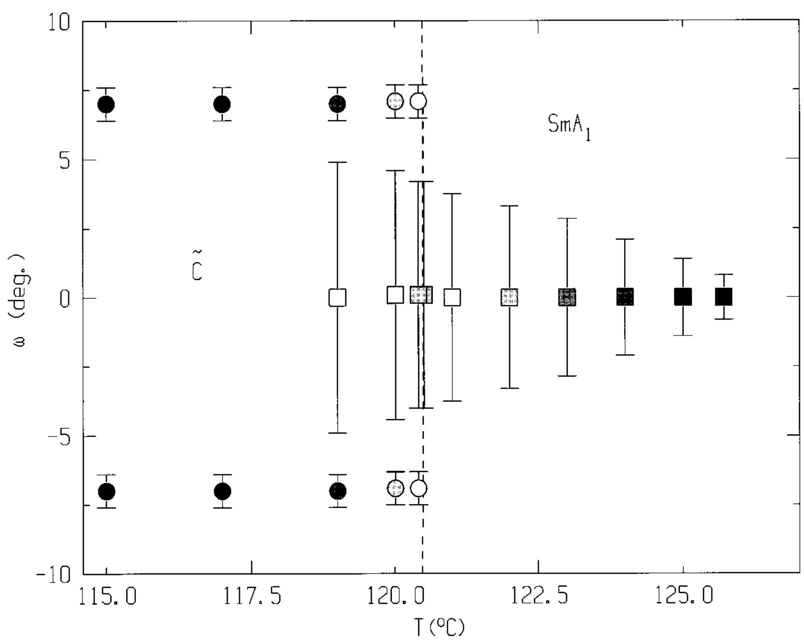


FIG. 10. Peak positions (circles and squares) and their full widths at half maximum (indicated by the error bars) of $2q_0$ scattering near the Sm-$A_1$–$\widetilde{C}$phase transition representing $\widetilde{C}$ and Sm-$A_1$ layer modulations. The gray scale of the circles and squares qualitatively indicates the intensities of quasi-Bragg and Bragg peaks.

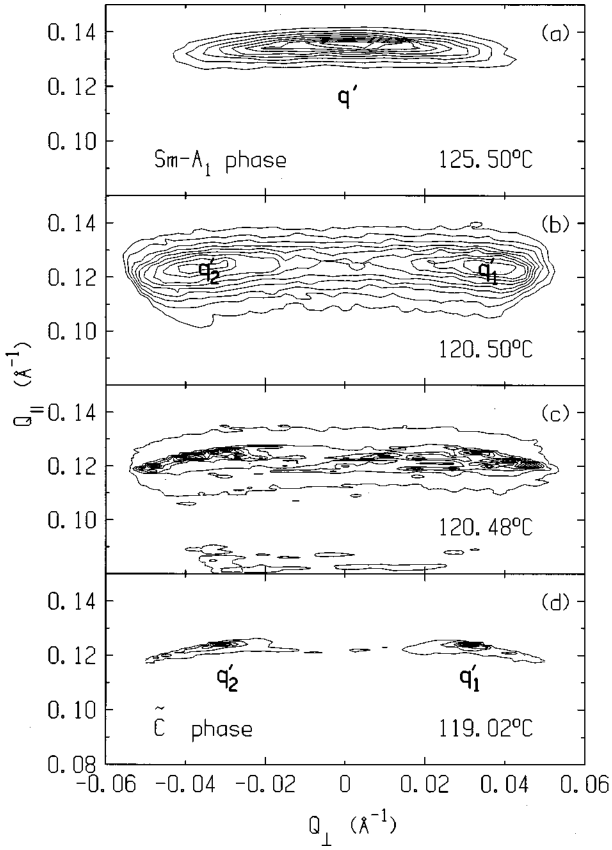


FIG. 11. Onset and temperature dependence of antiphase modulations indicated by changes in the $q'$ scattering. (a) In the Sm-$A_1$ phase, the diffuse $q'$ peak is due to the Sm-$A_d$ phase fluctuations. (b) The antiphase fluctuations gradually develop into off-axis diffuse scattering at $q_1'$ and $q_2'$. (c) Diffuse scattering due to broad mosaic arising from layer tilt. (d) Development of antiphase modulation is indicated by the condensation of $q_1'$ and $q_2'$ peaks. Note that only the $q_1'$ and $q_2'$ peaks are visible in the high-resolution results shown here. See the text for further details.

axis scattering moved to a slightly lower value of $Q_\parallel$ and the intensity increased as the Sm-$A_1$-$\widetilde{C}$ transition was approached, as shown in Fig. 11(b). At a slightly lower temperature, the incommensurate and antiphase fluctuations became equally pronounced, a specklelike diffraction pattern consisting of sharp peaks randomly distributed over the broad diffuse ring was observed for scattering near $q'$, as shown in Fig. 11(c). This diffraction pattern is not the x-ray speckle pattern that normally contains information about fluctuations within a single domain because of the poor transverse coherence length in our setup. This pattern is also not due to the mosaic of the sample since the scattering condensed into two Bragg peaks [Fig. 11(d)] at lower temperatures. A previous study [11] observed excess heat capacity in this region and attributed it to defects in polarization and mass-density orders and energy changes associated with the development of a long-range $\widetilde{C}$ polarization modulation. This diffraction pattern could be interpreted as being due to random phase shifts introduced by domain walls of the antiphase modulation. Initially, the tilt domains could be arranged in a zigzag pattern in compliance with the antiphase modulations because the antiphase fluctuations were stronger than the orientational fluctuations. The coexisting smectic-$A_1$ domains would then serve as domain walls between two adjacent antiphase tilted domains. The lateral size of the smectic-$A_1$ domains could be random, which would introduce random phase shifts. The tilted antiphase $\widetilde{C}$ domains grow at the cost of smectic-$A_1$ domains, as indicated by the evolution of the $2q_0$ peaks in Fig. 10. The on-axis peak gradually became a weaker peak as the tilted antiphase developed. An important requirement for generating such a specklelike diffraction pattern is the special attachment rules [19], such as those which apply to the antiphase domains in metallic alloys [20]. These rules have been met in our experiment by both the tilted and untilted domains since their directors were aligned by an external magnetic field.

The antiphase $\widetilde{C}$ fully developed at 119.02 °C [Fig. 11(d)] when the $q'$ peaks condensed into two pairs of Bragg peaks: $\mathbf{q}_1', \mathbf{q}_1'' = (2\mathbf{q}_0 - \mathbf{q}_1')$ with $2q_0 = (-0.025, 0, 0.204)$ Å$^{-1}$ for one pair and $\mathbf{q}_2', \mathbf{q}_2'' = (2\mathbf{q}_0 - \mathbf{q}_2')$ with $2q_0 = (+0.025, 0, 0.204)$ Å$^{-1}$ for the other. The *on-axis* $2q_0$ peak of the Sm-$A_1$ phase eventually vanished. The companion peaks at $(2\mathbf{q}_0 - \mathbf{q}_1')$ and $(2\mathbf{q}_0 - \mathbf{q}_2')$ are not seen in this figure because they lie outside our high-resolution experimental angular range. Their positions were determined later with a (low resolution) Siemens diffractometer.

Figure 12 shows the evolution of various peaks in the antiphase $\widetilde{C}$ with temperature. The lines of points $a$ and $a'$ represent changes in the position of off-axis peaks at $\mathbf{q}_1'$ and $\mathbf{q}_1'' = (2\mathbf{q}_0 - \mathbf{q}_1')$, respectively. The $2q_0$ scattering corresponding to this pair remained stationary. The projections of the incommensurate wave vector $\mathbf{q}_1'$ parallel and perpendicular to the smectic layer normal were $q_1' \cos\alpha$ and $Q_x = q_1' \sin\alpha$. Here, $\alpha$ (=22.1°) is the angle between $2\mathbf{q}_0$ and $\mathbf{q}_1'$ at 119.0 °C. The period of the antiphase modulation in the smectic plane was $2\pi/(|q_1'|\sin\alpha) = 130$ Å at 119 °C, and it increased with decreasing temperature with a fixed molecular tilt angle ($\gamma = 7°$). The average domain size increased nearly linearly with temperature as $\mathbf{q}_1'$ and $\mathbf{q}_1'' = (2\mathbf{q}_0 - \mathbf{q}_1')$ reflections tended to approach the one-dimensional lock-in position at $q_0$, indicated by the large open circle in Fig. 12. The period of the antiphase modulation attained a value of 237 Å before discontinuously jumping to infinity at the $\widetilde{C}$ − Sm-$A_2$ transition at 100.5 °C, as shown in the inset of Fig. 12. At the transition, positions of the peak at $\mathbf{q}_1'$ and $\mathbf{q}_1''$ discontinuously jump to the "on-axis" position indicated by the big open square. The complementary pair at $\mathbf{q}_2'$ and $\mathbf{q}_2''$, exhibiting a similar behavior, also jumps to the open square.

Figure 13 shows the longitudinal and transverse scans through the $q_1'$, $q_2'$, and $q_0$ peaks near the $\widetilde{C}$-$A_2$ transition. At 101.1 °C, the two antiphase peaks were at $(\pm 0.012, 0, 0.1085)$ Å$^{-1}$ with some diffuse scattering centered around (0,0,0.098) Å$^{-1}$. At 101.0 °C, the antiphase peaks moved closer towards $(\pm 0.010, 0, 0.1083)$ Å$^{-1}$. At temperature below 100.5 °C, a single on-axis condensed peak gradually developed from diffuse scattering. This peak is at (0, 0, 0.1025) Å$^{-1}$, commensurate with the on-axis part of the $2q_0$ peak at (0, 0, 0.205) Å$^{-1}$. These two on-axis commensurate peaks gained intensity at the expense of the off-axis peaks, indicating the advent of the bilayer Sm-$A_2$ phase. At 100.5 °C, the

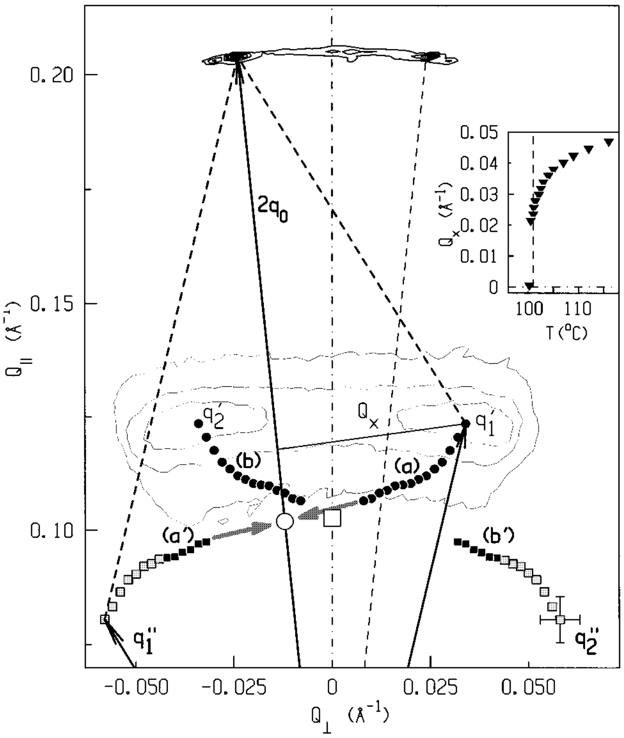

FIG. 12. Temperature dependence of the off-axis $\mathbf{q}_1'$, $\mathbf{q}_2'$, $\mathbf{q}_1'' = (2\mathbf{q}_0 - \mathbf{q}_1')$, $\mathbf{q}_2'' = (2\mathbf{q}_0 - \mathbf{q}_2')$ peaks and the on-axis $(2\mathbf{q}_0)$ peaks in the antiphase $\tilde{C}$. The $2q_0$ peaks remained stationary. The positions of anti-phase peaks indicated by lines of points $a$ and $b$ were measured at 119.0, 116.0, 112.0, 109.0, 107.0, 105.0, 104.0, 103.0, 102.5, 102.1, 101.4, 101.1, 101.0, and 100.5 °C. The shaded squares on lines $(a')$ and $(b')$ were obtained from a low resolution experiment in the same temperature range. Representative uncertainties in the values of the scattering vectors for these points are shown for one point. The $\mathbf{q}_1'$ and $\mathbf{q}_1''$ peaks moved towards $2\mathbf{q}_0/2$ (big open circle) but jumped to the position shown by the big open square at the transition to the Sm-$A_2$ phase. The vectors represent the positions of the scattering peaks in reciprocal space at 119.00 °C. The contour map is a plot of the $\tilde{C}$ fluctuations measured at 120.5 °C. Temperature dependence of the in-plane modulation, $Q_x$ is shown in the inset. At temperatures just below the transition (dashed line in the inset), peaks corresponding to the antiphase $\tilde{C}$ and Sm-$A_2$ phase were observed simultaneously.

single condensed peak, located now at (0, 0, 0.1030) Å$^{-1}$, coexisted with two diffuse antiphase peaks at ($\pm$0.008, 0, 0.1065) Å$^{-1}$. At 100.3 °C the two antiphase peaks disappeared. At the same temperature and after an equilibration time of about 10 min, $\omega$ scans of the peaks at $2q_0$ (=0.209 Å$^{-1}$) and $q_0$ (=0.1045 Å$^{-1}$) were found to be identical. The profiles of the quasi-Bragg peaks at both $2q_0$ and $q_0$ consisted of a strong on-axis peak and two off-axis peaks at $\omega = \pm 7°$. The intensity of the off-axis peaks started to increase with time at $T = 100.3$ °C, suggesting the development of the Sm-$C_2$ phase. Molecular tilt in the Sm-$C_2$ phase calculated from separation of peaks in $\omega$ scans increased with decreasing temperature. The intensity of the off-axis peaks also increased with a decrease in temperature. The tilt reached 14° at 87.5 °C. The system eventually crystallized at 87.3 °C. Since the bilayer smectic-$A_2$ phase appeared for a very narrow temperature range and is not very stable in nature, it could have been missed in previous calorimetric measurement [11] or in studies of less well aligned samples.

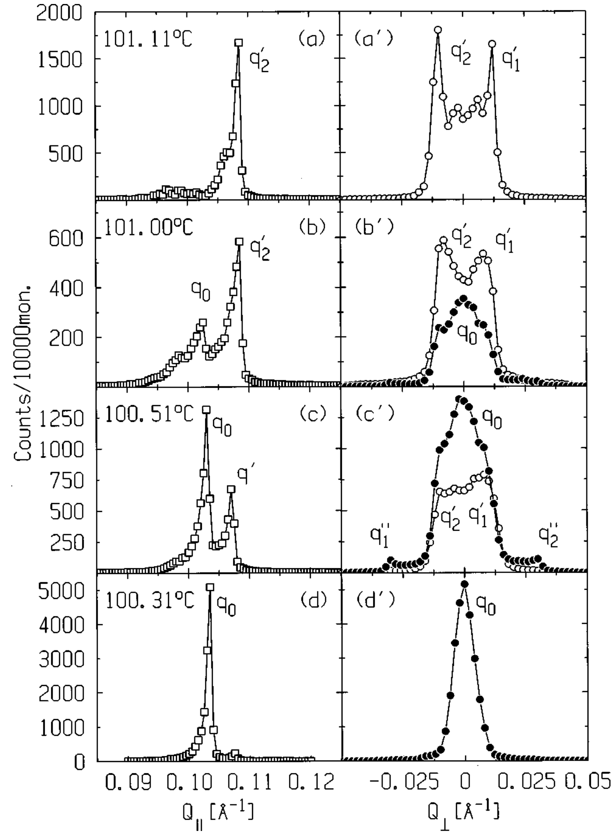

FIG. 13. Longitudinal and transverse scans of $q_1'$, $q_2'$, and $q_0$ scattering near the $\tilde{C}-$Sm-$A_2$ transition. Longitudinal scans shown were conducted at the highest peak positions shown in the transverse scans. (a) and $(a')$: the off-axis antiphase peaks. (b) and $(b')$: the off-axis antiphase peaks with a single on-axis condensed peak at $q_0$. (c) and $(c')$: the condensed peak at $q_0$ gained intensity while the antiphase peaks became diffuse with decreasing temperature. (d) and $(d')$: the off-axis antiphase peaks disappeared as the sample entered the Sm-$A_2$ phase.

## IV. CONCLUSIONS

Using high resolution x-ray diffraction, we have explored the smectic polymorphism and fluctuation effects in a mixture of octyl- and decyl-oxyphenyl nitrobenzoyloxy benzoate ($DB_8ONO_2 + DB_{10}ONO_2$) with 52.6 mol% of the decyl-homolog, a concentration below that for the Sm-$A_d-N-$Sm-$A_1$ triple point. The direct observation of a nematic-nematic $(N_d - N_1)$ phase transition in the narrow nematic estuary between the Sm-$A_d$ and Sm-$A_1$ phases is in accordance with the dislocation-loop melting theory of reentrant nematics with fluctuations taken into account. The development of lateral fluid antiphase fluctuations from the partial bilayer fluctuations in the monolayer Sm-$A_1$ phase has been probed and analyzed by analogy to the transition between Sm-$A$-like and Sm-$C$-like fluctuations using the Chen-Lubensky [13] model, and the uniaxial-biaxial fluctuation transition in this system was quantitatively determined. The undulations of the smectic layers in the Sm-$A_1$ phase and at the onset of the tilted antiphase $\tilde{C}$ were closely examined. The observation of an anomalous speckle-like diffraction pattern at the onset of the tilted antiphase indicated a delicate balance of the intermolecular interaction and thermal effects. The observed zigzag arrangement of $\widetilde{C}$ domains also indicated the delicate force balance in this incommensurate system. The transition between the tilted antiphase $\widetilde{C}$ and tilted bilayer Sm-$C_2$ phase was accompanied by a coexisting bilayer Sm-$A_2$ phase, which was not detected by calorimetric techniques [11].

## ACKNOWLEDGMENTS

The authors thank M. Sutton, P. Heiney, A. M. Levelut, and S. K. Sinha for helpful discussions, and acknowledge the use of the Siemens X1000 diffractometer at the characterization facility of the Liquid Crystal Institute. This research was supported by the NSF Science and Technology Center ALCOM Grant No. DMR-89-20147 and NSF Grant No. DMR-93-11853.

[1] G. Sigaud, F. Hardouin, and M. F. Achard, Phys. Lett. **72A**, 24 (1979); G. Sigaud, F. Hardouin, M. F. Achard, and H. Gasparoux, J. Phys. C (Paris), Colloq. **40**, C3-356 (1979).
[2] L. Longa and W. H. de Jeu, Phys. Rev. A **28**, 2380 (1983).
[3] J. Prost and P. Barois, J. Chim. Phys. Phys.-Chim. Biol. **80**, 65 (1983); P. Barois, J. Prost, and T. C. Lubensky, J. Phys. (Paris) **46**, 391 (1985).
[4] A. M. Levelut, R. J. Tarento, F. Hardouin, M. F. Achard, and G. Sigaud, Phys. Rev. A **24**, 2180 (1981).
[5] C. R. Safinya, W. A. Varady, L. Y. Chiang, and P. Dimon, Phys. Rev. Lett. **57**, 432 (1986).
[6] E. Fontes, P. A. Heiney, J. L. Haseltine, and A. B. Smith, III, J. Phys. (France) **47**, 1533 (1986).
[7] J. Prost and J. Toner, Phys. Rev. A **36**, 5008 (1987).
[8] V. N. Raja, R. Shashidhar, B. R. Ratna, G. Heppke, and Ch. Bahr, Phys. Rev. A **37**, 303 (1989).
[9] (a) J. O. Indekeu and A. Nihat Berker, Phys. Rev. A **33**, 1158 (1986); (b) J. O. Indekeu, A. Nihat Berker, C. Chiang, and C. W. Garland, *ibid.* **35**, 1371 (1987).
[10] G. Nounesis, S. Kumar, S. Pfeiffer, R. Shashidhar, and C. W. Garland, Phys. Rev. Lett. **73**, 565 (1994).
[11] (a) K. Ema, G. Nounesis, C. W. Garland, and R. Shashidhar, Phys. Rev. A **39**, 2599 (1989); (b) G. Nounesis, C. W. Garland, and R. Shashidhar, *ibid.* **43**, 1849 (1991).
[12] Y. Shi, G. Nounesis, and S. Kumar, Phys. Rev. E **54**, 1570 (1996).
[13] J. H. Chen and T. C. Lubensky, Phys. Rev. A **14**, 1202 (1976).
[14] R. Shashidhar, B. R. Ratna, V. Surendranath, S. Krishna Prasad, and C. Nagabhusan, J. Phys. (Paris), Lett. **46**, L-445 (1985).
[15] W. R. Busing and H. A. Levy, Acta Crystallogr. **22**, 457 (1967).
[16] L. J. Martinez-Miranda, A. R. Kortan, and R. J. Birgeneau, Phys. Rev. A **36**, 2372 (1987).
[17] C. W. Garland, in *Geometry and Thermodynamics*, edited by J.-C. Toledano (Plenum Press, New York, 1990), p. 221.
[18] M. J. Young, L. Wu, G. Nounesis, C. W. Garland, and R. J. Birgeneau, Phys. Rev. E **50**, 368 (1994).
[19] A. Garg and D. Levine, Phys. Rev. Lett. **60**, 2160 (1988); K. F. Ludwig, Jr., *ibid.* **61**, 1526 (1988).
[20] M. Sutton, S. G. Mochrie, T. Greytak, S. E. Nagler, L. E. Berman, G. A. Held, and G. B. Stephenson, Nature (London) **352**, 608 (1991).